Chinese Chemical Letters 36 (2025) 110199

Contents lists available at ScienceDirect

Chinese Chemical Letters

journal homepage: www.elsevier.com/locate/cclet

Synergistic enhancement of alkaline hydrogen evolution reaction by role of Ni-Fe LDH introducing frustrated Lewis pairs *via* vacancy-engineered

Mianfeng Li[a], Haozhi Wang[a,b,*], Zijun Yang[a], Zexiang Yin[a], Yuan Liu[b], Yingmei Bian[a], Yang Wang[a,*], Xuerong Zheng[a], Yida Deng[a,b,*]

[a] State Key Laboratory of Marine Resource Utilization in South China Sea, School of Materials Science and Engineering, Hainan University, Haikou 570228, China

[b] Tianjin Key Laboratory of Composite and Functional Materials, Key Laboratory of Advanced Ceramics and Machining Technology, (Ministry of Education), School of Materials Science and Engineering, Tianjin University, Tianjin 300072, China

ARTICLE INFO

Article history:
Received 27 May 2024
Revised 7 June 2024
Accepted 1 July 2024
Available online 3 July 2024

Keywords:
Ni-Fe LDH
Frustrated Lewis acid-base pair
Density functional theory
The *ab initio* molecular dynamics
The alkaline hydrogen evolution reaction

ABSTRACT

The alkaline hydrogen evolution reaction (HER) is a crucial process for sustainable hydrogen production, yet it requires efficient and stable electrocatalysts to overcome the high activation energy barrier. The article discusses a novel strategy for enhancing the performance of Ni-Fe layered double hydroxide (Ni-Fe LDH) in the alkaline HER by modifying it with a frustrated Lewis acid-base pair (FLP) constructed through vacancy engineering. The study found that the modified Ni-Fe LDH exhibited improved alkaline HER performance. Density functional theory (DFT) calculations demonstrate that the introduction of FLP can activate water and protons more efficiently than monometallic sites, thus reducing the alkaline HER energy barrier and overpotential. In HER under alkaline conditions, the Volmer step involves an additional hydrolysis dissociation compared to acidic conditions, which is one of the factors contributing to the slow reaction kinetics. This paper demonstrates that FLPs can alter the rate-determining step in alkaline HER from the Volmer step to a step with a lower energy barrier, more suitable for hydrogen desorption. The work provides new insights into the role of FLPs in regulating the mechanism and kinetics of HER and opens a new direction for the design and optimization of LDH-based and other electrocatalysts.

Hydrogen is a renewable and clean energy carrier with various applications, including fuel cells, power generation, and chemical synthesis [1]. However, current hydrogen production methods primarily rely on fossil fuels, leading to environmental pollution and greenhouse gas emissions [2]. Therefore, developing efficient and sustainable hydrogen production technologies is crucial for the energy and environmental sectors [3]. Water electrolysis emerges as a promising method for hydrogen production, converting water into hydrogen and oxygen using electricity from renewable energy sources such as solar, wind, and hydroelectric power. This method produces high-purity hydrogen without any polluting byproducts [4]. There are two main categories of hydrogen production from electrolyzed water: alkaline and acidic. The alkaline hydrogen evolution reaction (HER) is an attractive option due to its low cost, low susceptibility to corrosion, and the potential for industrial mass production [5]. However, challenges remain for alkaline HER. The materials used in alkaline water electrolysis for hydrogen production still depend on precious metals like platinum and iridium [6]. While these metals exhibit excellent activity, their scarcity and expense limit large-scale application [7]. Non-precious metal catalysts, including metal alloys, metal oxides, metal sulfides, metal phosphides, metal nitrides, and metal carbides, suffer from low activity, poor stability, or complex synthesis processes [8]. Thus, developing low-cost and high-performance electrocatalysts for alkaline water electrolysis is essential for promoting hydrogen production and utilization [9].

Among the various electrocatalysts for alkaline water electrolysis, layered double hydroxides (LDHs) have emerged as a new class of non-noble metal catalysts, owing to their unique structural and chemical properties [10]. LDHs belong to a family of two-dimensional (2D) materials with a general formula of $[M(II)_{1-x}M(III)_x(OH)_2]^{x+}(A^{n-})_{x/n}\cdot mH_2O$, where M(II) and M(III) are divalent and trivalent metal cations, respectively; An- is an interlayer anion; and m represents the number of water molecules [11].

* Corresponding author.
E-mail addresses: hzwang001@hainanu.edu.cn (H. Wang), yangwangwy@hainanu.edu.cn (Y. Wang), yd_deng@hainanu.edu.cn (Y. Deng).

https://doi.org/10.1016/j.cclet.2024.110199
1001-8417/

LDHs possess a positively charged brucite-like layer and a negatively charged interlayer, forming a natural electric double layer that can facilitate the adsorption and activation of water molecules and protons [12]. Among various LDHs, Ni-Fe-layered double hydroxide (Ni-Fe LDH) is known as an effective electrocatalyst for the oxygen evolution reaction (OER) in alkaline media, due to its high activity, stability, and earth-abundance [13]. The high OER activity of Ni-Fe LDH is mainly attributed to the synergistic effect between Ni and Fe atoms [14]. However, its slow alkaline HER process greatly limits its practical application. Recent studies have reported that Ni-Fe LDH can exhibit a dual function for alkaline HER/OER when its composition, structure, and morphology are rationally controlled [15]. However, the reaction mechanism and kinetic explanation for its excellent performance remain unclear, as computational modeling considering only hydrogen adsorption is inadequate. It is widely accepted that the study of alkaline HER requires consideration of the effects of water adsorption energy, water activation energy, and hydroxide adsorption energy, in addition to the hydrogen adsorption energy [16]. This is due to the existence of an extra water dissociation energy barrier in the Volmer step, which causes slow kinetics of alkaline HER since H^* protons can only come from the hydrolysis dissociation process. Based on this, the strategy naturally considered when designing catalysts is to create synergistic dual active sites. Ni-Fe LDH is a promising electrocatalyst, as it has abundant and active metal sites that can facilitate water splitting reactions [14]. At the same time, the role of oxygen sites, such as hydroxyl groups in Ni-Fe LDH, is often overlooked; they may also participate in the alkaline HER process and enhance catalytic performance [17]. By investigating and modifying the oxygen sites in Ni-Fe LDH [18], we can optimize their interaction with the metal sites [19], and improve their electronic structure and activity for the alkaline HER [20]. Therefore, the oxygen sites in Ni-Fe LDH are crucial for achieving efficient and low-cost hydrogen production from alkaline water electrolysis.

Frustrated Lewis pairs (FLPs) are non-homogeneous catalysts composed of Lewis acids (LA) and Lewis bases (LB) [21]. They are spatially hindered from forming classical Lewis adducts, leading to strong interactions between LA and LB. FLPs are widely used as catalysts for various reactions, including hydrogenation, dehydrogenation, and CO_2 reduction, due to their ability to activate small molecules such as H_2 [22], SO_2 [23], N_2O [24], and CO_2 [25]. FLPs can modify the electronic structure and reactivity of substrates and offer multiple active sites for reactions [26]. Researchers have recently utilized OH defects on AlOOH layers to create Lewis acidic Al^{3+} sites and Lewis basic OH_v sites, forming solid frustrated Lewis acid-base pairs [27]. Based on the innovative design of AlOOH-based FLPs, a new approach has been conceived for the incorporation of FLP sites into Ni-Fe LDH to strategically enhance the alkaline HER performance. The rationale behind this design is the potential of FLPs to introduce a synergistic effect within the Ni-Fe LDH matrix, thereby optimizing its electronic properties and catalytic activity.

In this work, we propose a novel strategy to enhance the HER performance of Ni-Fe LDH by modifying it with FLPs. We hypothesize that FLPs can synergistically enhance the HER activity of Ni-Fe LDH by creating more active sites, improving electrical conductivity, and facilitating proton transfer. To test this hypothesis, we utilized density-functional theory (DFT) calculations to create FLPs by constructing hydroxide vacancies at the O site with the acidic site as Ni and the basic site as the O site (with H removed). The corresponding basic HER properties were then systematically explored for both pristine Ni-Fe LDH and FLP-modified Ni-Fe LDH engineered with O vacancies. We found that FLP-modified Ni-Fe LDH exhibited significantly enhanced HER activity, stability, and kinetics compared to both FLP-unmodified and pristine Ni-Fe LDH.

All calculations were performed using the Vienna ab initio Simulation Package (VASP) code [28] with the Perdew-Burke-Ernzerhof (PBE) functional [29] and the plane-wave DFT method. Electron-ion interactions were described using the projector augmented wave (PAW) method [30]. A plane-wave cutoff energy of 400 eV was used for all calculations, with a convergence threshold of 10^{-5} eV in energy and −0.01 eV/Å in force. To prepare for further doping, we constructed a $2 \times 1 \times 1$ supercell of the FLP-LDH monolayer. The optimized structure resulted in superlattice dimensions of $a = 12.3964$ Å and $b = 10.7379$ Å. To minimize interaction between periodic images, we inserted a vacuum space of 15 Å in the z-direction. We used a $2 \times 2 \times 1$ grid for the repetitive unit by the Monkhorst–Pack scheme to obtain k-point sampling of the Brillouin zone. For the density of state (DOS) calculations, we employed the finer $5 \times 4 \times 1$ k-points grid to achieve higher accuracy. Additionally, we employed the empirical DFT-D3 correction to improve the van der Waals interaction [31]. We also performed the DFT + U method to correct for the artificial electron self-interaction for 3d orbitals of transition metals [32]. The values of U-J were set as 4.0 eV and 6.0 eV for Fe and Ni, respectively [33].

To evaluate the theoretical HER performance of a catalyst under alkaline conditions, four elementary steps were considered in our work:

$$* + H_2O \rightarrow H_2O^* \tag{1}$$

$$H_2O^* \rightarrow H^* + OH^* \tag{2}$$

$$H^* + OH^* + e^- \rightarrow H^* + OH^- \tag{3}$$

$$H^* \rightarrow * + \frac{1}{2}H_2 \tag{4}$$

Eqs. 1 and 2 represent the water adsorption and water activation steps, respectively, followed by the desorption of OH^* (Eq. 3) and H_2 production (Eq. 4). The thermodynamic analysis of these steps was based on the computational standard hydrogen electrode (CHE) model developed by the groups of Nørskov and Rossmeisl [34]. The change in Gibbs free energy for each reaction (ΔG_1, ΔG_2, ΔG_3, ΔG_4) can be calculated as follows [35].

$$\Delta G_1 = G_{H_2O^*} - G_{H_2O(l)} \tag{5}$$

$$\Delta G_2 = G_{H^*} + G_{OH^*} - G_{H_2O^*} \tag{6}$$

$$\Delta G_3 = G_{H_2O(l)} - G_{OH^*} - \frac{1}{2}G_{H_2} + \Delta G_U + \Delta G_{pH} \tag{7}$$

$$\Delta G_4 = \frac{1}{2}G_{H_2} - G_{H^*} \tag{8}$$

The calculation of Gibbs free energies (G) involves considering both enthalpy and entropy corrections. A detailed calculation method for Gibbs free energy is presented in Supporting information. Additionally, ΔG_U and ΔG_{pH} are terms used for the bias effect and pH correction, respectively, and can be calculated as follows [36]:

$$\Delta G_U = -eU \tag{9}$$

$$\Delta G_{pH} = -kT \ln[H^+] = kT \ln 10 \times pH \tag{10}$$

The electrode potential relative to the standard hydrogen electrode (SHE) is represented by U, while k and T represent the Boltzmann constant and temperature, respectively. In this case, the

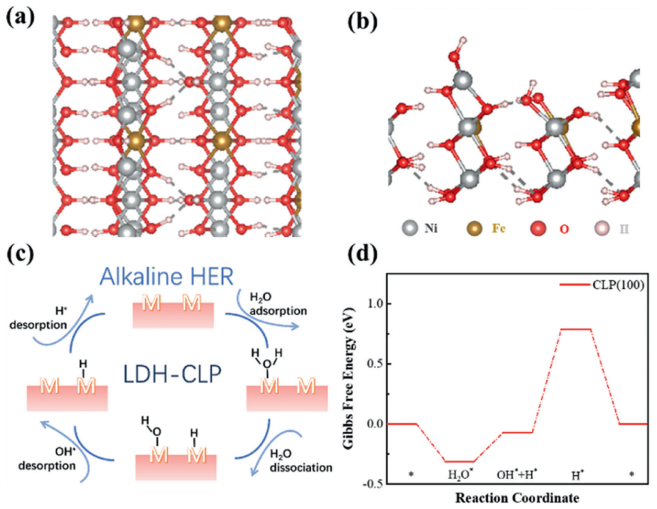

Fig. 1. (a) Top view, (b) side view of the surface crystal structure of CLP (100). For the model, the red, white, gray, and brown balls represent O atoms, H atoms, Ni atoms, and Fe atoms, respectively. (c) The proposed HER mechanism in alkaline solution. (d) Free energy diagram of alkaline HER on Ni-Fe LDH at electrode $U = 0.826$ V *vs.* SHE.

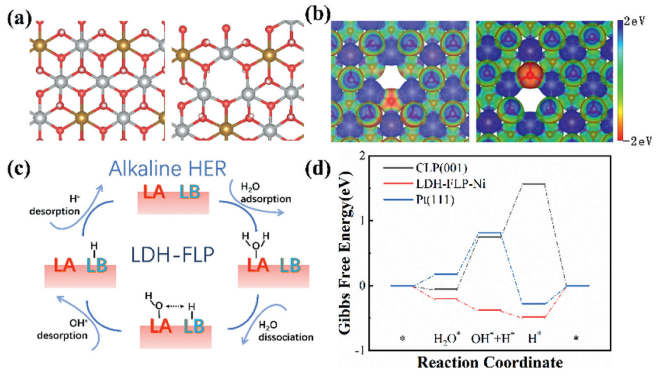

Fig. 2. (a) Structure of Ni-Fe LDH CLP(001) face; FLP-Ni, constructed with hydroxide and hydrogen ion vacancies, is the structure of Ni-Fe LDH (001) face after the introduction of FLP, with Ni site as Lewis acidic site and O site as Lewis basic site; its ESPs are shown in (b) main view, reverse orientation main view. (c) The proposed HER mechanism for FLP in alkaline solution, (d) Pt(111), CLP, FLP-Ni, their Gibbs free energy diagrams.

value of U at pH 14 was determined to be 0.828 V *versus* SHE, according to the Nernst equation [34]. Therefore, a negative ΔG value indicates that the corresponding reaction can occur spontaneously.

To determine the kinetic barrier of water dissociation, we utilized the climbing image nudged elastic band (CI-NEB) method to construct minimum energy paths (MEPs) [37]. The initial state (IS) was the adsorption of water molecules, while the final state (FS) was the adsorption of $OH^* + H^*$ pairs, which served as the endpoint of the water activation reaction. The transition state (TS) was determined using vibrational frequency analysis, confirmed by the unique negative eigenvalue of the Hessian matrix for the corresponding structure at the TS. The water activation barrier (G_a) can then be calculated using Eq. 11.

$$G_a = G_{TS} - G_{IS} \tag{11}$$

G_{TS} and G_{IS} represent the free energy of the transition state and initial state, respectively. A small G_a theoretically suggests a fast rate of water activation during the catalytic reaction.

Firstly, we chose the Ni-Fe LDH (100) surface, which exposes Ni sites as catalytic sites, as shown in Figs. 1a and b. The alkaline HER reaction mechanism is depicted in Fig. 1c, and the Gibbs energy diagram of alkaline HER was calculated to determine its properties. As shown in Fig. 1d, the theoretical overpotential of Ni-Fe LDH is 0.865 eV, and the rate-determining step for alkaline HER is hydroxyl desorption. The ΔG value for water adsorption is −0.312 eV, indicating that the water adsorption step is spontaneous. However, the energy of the hydrolysis dissociation step showed an increasing trend and the hydroxyl group after hydrolysis dissociation was difficult to desorb, leading to active site poisoning. This has been experimentally shown to be consistent; that is, many Ni-Fe LDHs perform well in OER catalysis, but their catalytic activity in HER is not so good. Therefore, we should further regulate the interaction between adsorbates and catalytic sites to improve the performance of alkaline HER.

We note that for basic HER, the high overpotential of Ni-Fe LDH is attributed not only to the high desorption energy of the hydroxyl group, but also to the lack of other catalytic sites that could facilitate water splitting. Subsequently, we calculated the Gibbs free energies of the basic HERs on the Ni-Fe LDH (001) and Pt (111) facets. We found that the decisive step for the Ni-Fe LDH (001) facet is 0.823 eV, while for the Pt (111) facet, it is 0.642 eV. Although the decisive step for the Ni-Fe LDH (001) facet, acting as a conventional Lewis acid-base pair (CLP), is greater than that of the reference Pt(111) facet, its water adsorption energy is not significantly high. Furthermore, based on the Ni-Fe LDH (001) facet, the arrangement of metal and oxygen sites is conducive to the formation of FLP. Thus, As shown in Fig. 2a, we introduced vacancies for hydroxide and hydrogen ions through vacancy engineering, thereby incorporating FLP. As shown in Fig. 2b, the Ni-O potential difference in the ESP diagram indicates that the FLP was successfully constructed. And the alkaline HER reaction mechanism is depicted in Fig. 2c. As shown in Fig. 2d, the results demonstrate that with the introduction of a suitable catalytic site, the hindered Lewis acid-base pair (FLP-Ni) exhibits improved catalytic performance in alkaline HER, with a rate-determining step of 0.485 eV, which is lower than that of the reference Pt(111) with a rate-determining step of 0.640 eV. Both its water adsorption and hydrolysis steps corresponded to thermodynamic decreases, with corresponding ΔG values of −0.201 eV, −0.176 eV. Thus, FLP-Ni is capable of spontaneously cleave water based on the moderate energy of the adsorbate, and the theoretical overpotentials are even lower than those of Pt (111). As shown in Figs. S5 and S6 (Supporting information), we calculated the Gibbs free energies of the ions containing their intercalation layers, which show a similar trend. Furthermore, as shown in Figs. S7 and S8 (Supporting information), we calculated the Gibbs free energy of LDH-FLP-Fe, whose rate-determining step energy is larger than that of the FLP-Ni site. This suggests that in FLP-Ni, the FLP (Ni-O) not only provides the catalytic site but also activates water molecules. These two factors synergistically contribute to intrinsic catalytic activity towards basic HER.

To better understand the interactions between the catalytic sites of LDH-FLP, we analyzed its differential charge density and density of states, with the results presented in Fig. 3. The differential charge density plot (Fig. 3a) illustrates a decrease in electrons around the Ni ion, acting as a Lewis acid, and an accumulation of electrons around the O ion, acting as a Lewis base. This demonstrates a clear tendency for electron mobility within this localized range of FLP (Ni-O). The density of states diagram (Fig. 3b) reveals that the Ni and O ions in the LDH-FLP material exhibit semiconducting properties with small gaps on either side of the Fermi energy level. The Lewis acid Ni ions in FLP (Ni-O) exhibit spikes above the Fermi energy level, while the Lewis base O ions in FLP (Ni-O) show spikes primarily below the Fermi energy level. This suggests the presence of an empty electron orbital for Ni ions and an occupied electron orbital for O ions, confirming the successful construction of FLP and the presence of a local charge imbalance.

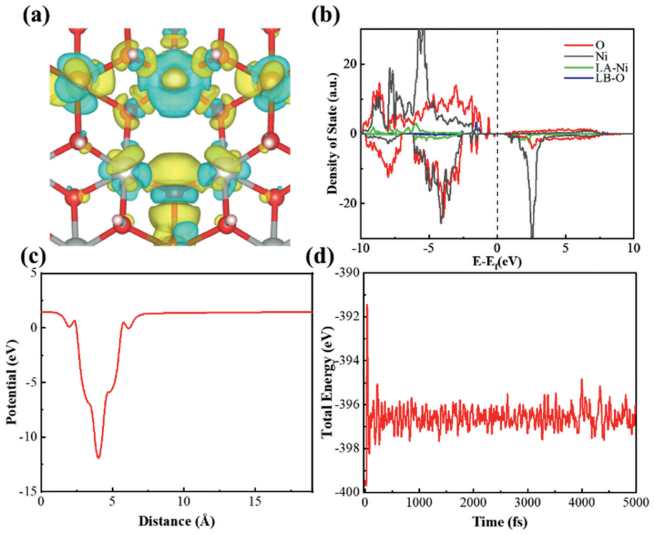

Fig. 3. (a) Differential charge diagram of FLP-Ni. (b) DOS diagram of FLP-Ni. In the figure, O and Ni represent O element and Ni element respectively, LB-O and LA-Ni respectively represent FLP (Ni-O) O atoms, Ni atoms. (c) Work function diagram of FLP-Ni. (d) AIMD diagram of FLP-Ni.

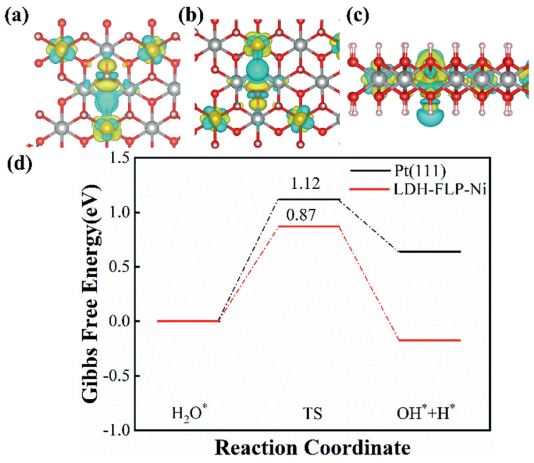

Fig. 4. (a) Top view, (b) inverted top view, (c) side view of LDH-FLP activated water structure. (d) Pt(111) surface, the water molecule of LDH-FLP dissociates the transition state energy barrier.

This imbalance can promote water cleavage and provide a catalytic site for the cleaved intermediates, thereby improving the performance of basic HERs. The work function, depicted in Fig. 3c, has a value of 1.98 eV, indicating that the material is readily capable of electron emission. To evaluate the cycling performance of the LDH-FLP material, we conducted AIMD calculations and observed that it maintains its energy stability after 5000 fs of cycling.

In addition, to probe the charge transfer of LDH-FLP during water activation in alkaline HER, we further examined its charge density difference upon water molecule activation (Fig. 4). The results revealed that for LDH-FLP, the metal atom Ni, acting as a Lewis acid, would accept electrons from hydroxide ions, displaying a yellow charge aggregation state (Fig. 4a). Meanwhile, the O atom, acting as a Lewis base, would attract electron-deficient hydrogen ions, displaying a yellow charge reduction state (Fig. 4b). This phenomenon aligns with our view that the hindered Lewis acid accepts electrons from the water molecule, while some electrons from the Lewis base attack the water molecule's antibonding orbitals, promoting the adsorption and activation of water. Further, FLP (Ni-O) provides a stable catalytic attachment site

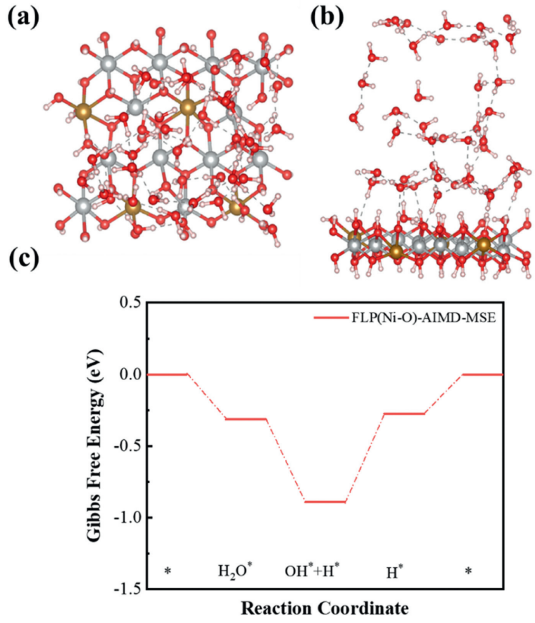

Fig. 5. (a) Top view, (b) side view of LDH-FLP-Ni dominant solvation model. (c) Gibbs free energy diagrams made by AIMD for the dominant solvation model, and red representing the mean stable energy (MSE).

for the activated product, crucial for stable and efficient catalysis. Beyond thermodynamic considerations, studying the hydrolysis dissociation process from a kinetic perspective is equally important. We further calculated the water activation energy barrier (E_a) for the LDH-FLP model using the optimized models of adsorbed and activated water molecules as the initial state (IS) and final state (FS), respectively, and employed the climbing image nudged elastic band method to identify the transition state (TS). As depicted in Fig. 4d, the optimized Gibbs energy diagrams for water molecule dissociation on the Pt (111) surface and LDH-FLP indicate that the water activation potential barriers are 1.12 eV for both surfaces, consistent with the thermodynamic results and the Brønsted-Evans- Polanyi (BEP) correlation rule [38].

Based on the alkaline HER mechanism study described above, we calculated the Gibbs free energy of dominant solvation for LDH-FLP-Ni using ab initio molecular dynamics (AIMD) results. The AIMD simulation was conducted at 300 K with a time step of 1 fs and a total simulation time of 5 ps in the NVT system. The structure is illustrated in Figs. 5a and b. Following the AIMD modeling, a 13 Å water layer stabilized above FLP-LDH–Ni. The reaction energies (Fig. 5c) indicate that both the interfacial water adsorption and water activation steps of the dominant solvation model during the AIMD process are exothermic. This suggests that the Volmer step, commonly perceived as the rate-determining step, can proceed spontaneously, thus shifting the rate-determining step to the desorption step-a trend similar to the reaction energy of the non-solvated model previously described. In addition, as shown in Figs. S9-S12, Video S1 and S2 (Supporting information), we considered two models and show their AIMD trajectories in as a way to investigate their stability in real solutions. Besides, as shown in Figs. S13-S15 (Supporting information), we did Gibbs free energy calculations with both methods.Similarly, as a comparison sample (Figs. S16 and S17 in Supporting information), the Gibbs free energy of Pt(111) in the dominant solvation model was considered, which confirms the better catalytic performance of LDH-FLP-Ni in the basic HER mechanism.

In summary, we conducted a comprehensive study on the catalytic design of Ni-Fe LDH for alkaline HER using DFT calcula-

tions, constructing a suitable FLP through vacancy engineering to exploit the FLP's property for small molecule activation, achieving efficient water adsorption and activation. Our calculations indicate that LDH-FLP-Ni is a stable and efficient alkaline HER electrocatalyst that significantly reduces the reaction energy barrier, resulting in a lower theoretical overpotential of 0.485 eV. The introduction of the superior co-catalytic site, FLP(Ni-O), with its unique property for small-molecule activation, can activate water molecules and protons more efficiently than purely metal site, thereby reducing the overpotential. Moreover, it was found that the FLP (Ni-O) active site can shift the rate-determining step in alkaline HER from the Volmer step, which is typically considered the determinant hindering alkaline HER activity, to a lower energy barrier. This work provides new insights into the enhanced role of FLP in regulating the mechanism and kinetics of alkaline HER and opens a new avenue for the design and optimization of LDH-based and other electrocatalytic materials.

Declaration of competing interest

The authors state that they have no competing financial interests or personal relationships that could have influenced the work reported in this paper.

CRediT authorship contribution statement

Mianfeng Li: Writing – original draft, Formal analysis, Data curation. **Haozhi Wang:** Writing – review & editing, Supervision, Methodology, Funding acquisition. **Zijun Yang:** Investigation. **Zexiang Yin:** Investigation. **Yuan Liu:** Investigation. **Yingmei Bian:** Investigation. **Yang Wang:** Investigation. **Xuerong Zheng:** Investigation. **Yida Deng:** Supervision, Funding acquisition.

Acknowledgments

This work was financially supported by National Natural Science Foundation of China (Nos. 52301011, 52231008, 52142304, 52177220, U23A200767, 52302236, and 22369005), Hainan Provincial Natural Science Foundation of China (Nos. 524QN226 and 524QN222), the Key Research and Development Program of Hainan Province (No. ZDYF2022GXJS006), Starting Research Fund from the Hainan University (No. KYQD (ZR)23026), International Science & Technology Cooperation Program of Hainan Province (No. GHYF2023007). We gratefully acknowledge HZWTECH for providing computation facilities.

Supplementary materials

Supplementary material associated with this article can be found, in the online version, at doi:10.1016/j.cclet.2024.110199.

References

[1] D. Guan, B. Wang, J. Zhang, et al., Energy Environ. Sci. 16 (2023) 4926–4943.
[2] M. Luo, Y. Yi, S. Wang, et al., Renew. Sustain. Energy Rev. 81 (2018) 3186–3214.
[3] A.I. Osman, N. Mehta, A.M. Elgarahy, et al., Environ. Chem. Lett. 20 (2022) 2213.
[4] P. Wang, Y. Chen, Y. Teng, et al., Renew. Sustain. Energy Rev. 194 (2024) 114303.
[5] J. Wei, M. Zhou, A. Long, et al., Nano-Micro Lett. 10 (2018) 1–15.
[6] G. Gao, G. Zhu, X. Chen, et al., ACS Nano 17 (2023) 20804–20824.
[7] G. Gao, G. Zhao, G. Zhu, et al., Chin. Chem. Lett. 36 (2025) 109557.
[8] S. Anantharaj, S. Noda, V.R. Jothi, et al., Angew. Chem. Int. Ed. 60 (2021) 18981–19006.
[9] C. Huang, J. Zhou, D. Duan, et al., Chin. J. Catal. 43 (2022) 2091–2110.
[10] D.D.A. de Fatima Palhares, L.G. Martins Vieira, J.J. Ribeiro Damasceno, Int. J. Hydrogen Energy 43 (2018) 4265–4275.
[11] Y. Cao, D. Zheng, F. Zhang, et al., J. Mater. Sci. Technol. 102 (2022) 232–263.
[12] Y. Feng, X. Wang, J. Huang, et al., Chem. Eng. J. 390 (2020) 124525.
[13] Y. Wang, S. Tao, H. Lin, et al., Nano Energy 81 (2021) 105606.
[14] H. Gu, G. Shi, H.C. Chen, et al., ACS Energy Lett. 5 (2020) 3185–3194.
[15] Y.J. Lee, S.K. Park, Rare Met. 43 (2024) 522–532.
[16] X. Wang, Y. Zheng, W. Sheng, et al., Mater. Today 36 (2020) 125–138.
[17] L. Chen, H. Zhang, L. Chen, et al., J. Mater. Chem. A 5 (2017) 22568–22575.
[18] D. Wang, Y. Jiao, W. Shi, et al., Prog. Mater. Sci. 133 (2023) 101055.
[19] D. Wang, J. Yu, X.B. Yin, et al., Natl. Sci. Rev. 10 (2023) nwad010.
[20] N. Lingappan, I. Jeon, W. Lee, J. Mater. Chem. A 11 (2023) 17797–17809.
[21] D.W. Stephan, Science 354 (2016) aaf7229.
[22] K. Chernichenko, A. Madarasz, I. Papai, et al., Nat. Chem. 5 (2013) 718–723.
[23] M. Sajid, A. Klose, B. Birkmann, et al., Chem. Sci. 4 (2013) 213–219.
[24] E. Otten, R.C. Neu, D.W. Stephan, J. Am. Chem. Soc. 131 (2009) 9918–9919.
[25] A.E. Ashley, A.L. Thompson, D. O'Hare, Angew. Chem. Int. Ed. 48 (2009) 9839–9843.
[26] Z.Q. Huang, T.H. Li, B. Yang, et al., Chin. J. Catal. 41 (2020) 1906–1915.
[27] S. Liu, M. Dong, Y. Wu, et al., Nat. Commun. 13 (2022) 2320.
[28] G. Kresse, J. Furthmuller, Phys. Rev. B 54 (1996) 11169–11186.
[29] J.P. Perdew, K. Burke, M. Ernzerhof, Phys. Rev. Lett. 77 (1996) 3865–3868.
[30] G. Kresse, D. Joubert, Phys. Rev. B 59 (1999) 1758–1775.
[31] S. Grimme, J. Comput. Chem. 27 (2006) 1787–1799.
[32] S.L. Dudarev, G.A. Botton, S.Y. Savrasov, et al., Phys. Rev. B 57 (1998) 1505.
[33] L. Wang, T. Maxisch, G. Ceder, Phys. Rev. B 73 (2006) 195107.
[34] J.K. Norskov, J. Rossmeisl, A. Logadottir, et al., J. Phys. Chem. B 108 (2004) 17886–17892.
[35] Y. Li, Y. Guo, S. Yang, et al., ACS Appl. Mater. Interfaces 13 (2021) 5052–5060.
[36] H. Xu, D. Cheng, D. Cao, et al., Nat. Catal. 1 (2018) 632.
[37] G. Henkelman, H. Jónsson, J. Chem. Phys. 113 (2000) 9978–9985.
[38] T. Bligaard, J.K. Nørskov, S. Dahl, et al., J. Catal. 224 (2004) 206–217.